

Design of Nanocellulose Fibrils Containing Lignin Segment (L-NCF) for Producing Stable Liquid Foams as “Green” Flooding Agents for Oil Recovery

Bing Wei,^{*,†,§} Yuanyuan Wang,[†] Runxue Mao,[†] Xingguang Xu,[‡] Colin Wood,^{‡,§} and Yangbing Wen^{||}

[†]State Key Laboratory of Oil and Gas Reservoir Geology and Exploitation, Southwest Petroleum University, 8 Xindu Avenue, Xindu District, Chengdu, Sichuan 610500, China

[‡]Energy Business Unit, The Commonwealth Scientific and Industrial Research Organization, 26 Dick Perry Avenue, Kensington 6152, Perth Australia

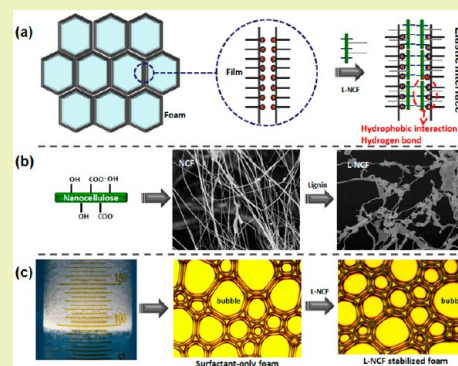
[§]Curtin Oil and Gas Innovation Centre (COGIC), Curtin University, Kensington 6151, Australia

^{||}Tianjin Key Laboratory of Pulp and Paper, Tianjin University of Science & Technology, 29 No. 13 Street, Economy and Technology Development, Tianjin, 300457, China

Supporting Information

ABSTRACT: Foam stability is a crucial consideration in the view of its numerous applications. Herein, a series of nanocellulose fibrils containing lignin segment (L-NCF) was designed and then utilized for interfacial stabilization of liquid foams for eco-friendly oil recovery applications. The ability to form foams and their stability at bulk scale and bubble scale were thoroughly investigated using a foam scanner. Liquid drainage rate, bubble rupture, interfacial dilational viscoelasticity, and bubble transport in porous media were studied as a function of lignin content. We observed that in a vertical column the addition of L-NCF significantly mitigated the drainage of the liquid foams. The foam volume stability (FVS) index indicated that the stability of the foams in the presence of L-NCF was up to five times higher than that of surfactant-only foam. The hydrophobic interaction between the surfactant (mixture of alkyl polyglycoside (APG) and anion surfactant alpha olefin sulfonate (AOS)) and L-NCF (lignin segment) constructed an elastic interface for the foams, which notably protected the liquid foams from coarsening and coalescence. The L-NCF stabilized foams can appropriately transport in porous media without the plugging issue, during which great differential pressures are simultaneously built up as a result of the yielded elastic interface. It is believed that nanocellulose is very promising in the oil production industry as a green alternative to synthetic chemicals.

KEYWORDS: Foam stability, Air water interface, Nanocellulose fibrils, Lignin, Enhanced oil recovery



INTRODUCTION

Liquid foam is essentially a nonequilibrium soft matter usually produced by bubbling gas in a solution containing surface-active agents, in which liquid is the continuous phase with gas phase trapped in thin liquid films.¹ Foams have been widely used in numerous areas such as flotation, dust control, fire control, food processing, and personal care products for many decades, and they have been applied in oil production.^{2–6} It has been recognized that for a given reservoir primary and secondary recovery methods merely account for less than 40% of the original oil in place (OOIP). The depletion of the majority of the oilfields worldwide coupled with the growing energy consumption spurred the research efforts on enhanced oil recovery (EOR) technologies to further promote the oil recovery. Therefore, foam-EOR has been rapidly growing in recent years.

Despite the advantages of foams, a major issue for this technology is the foam stability in deep reservoirs (with high

temperature and pressure) especially when crude oil is present since quite a few reports have observed the detrimental effect of hydrocarbons on foam stability.^{7–14} Furthermore, surfactants are prone to detach from the bubble surface when foams are subjected to high-temperature and salinity.^{15–17} As reported, the foam stability is heavily dependent on bulk and surface viscosities, micelle concentration, disjoining pressure, hydrophobic interactions, surface tension (equilibrium and dynamic), and surfactant adsorption at the air/water interface. On the basis of these mechanisms, substantial efforts have been made in the past decades aiming to boost foam stability and extend foam longevity in reservoirs.

Received: March 3, 2019

Revised: June 2, 2019

Published: June 10, 2019

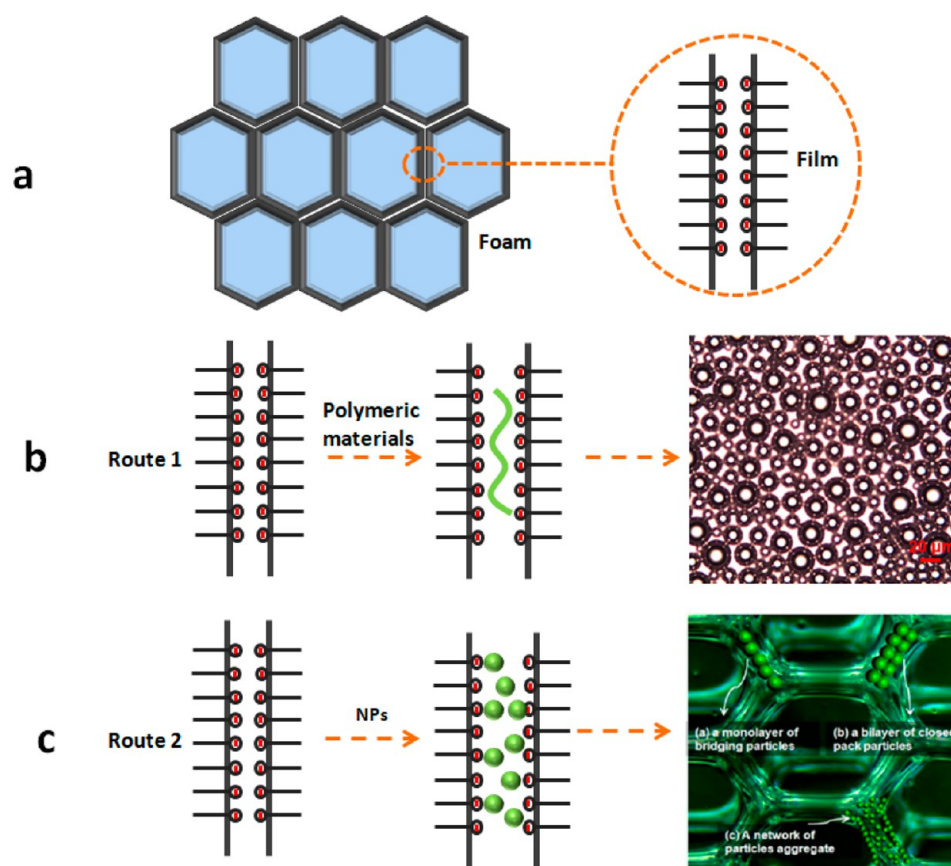


Figure 1. Stabilization of foam film using NPs and polymeric materials. Figure partially adapted from ref 24, copyright 2015 American Chemical Society, and partially adapted with permission from ref 27, copyright 2015 Elsevier.

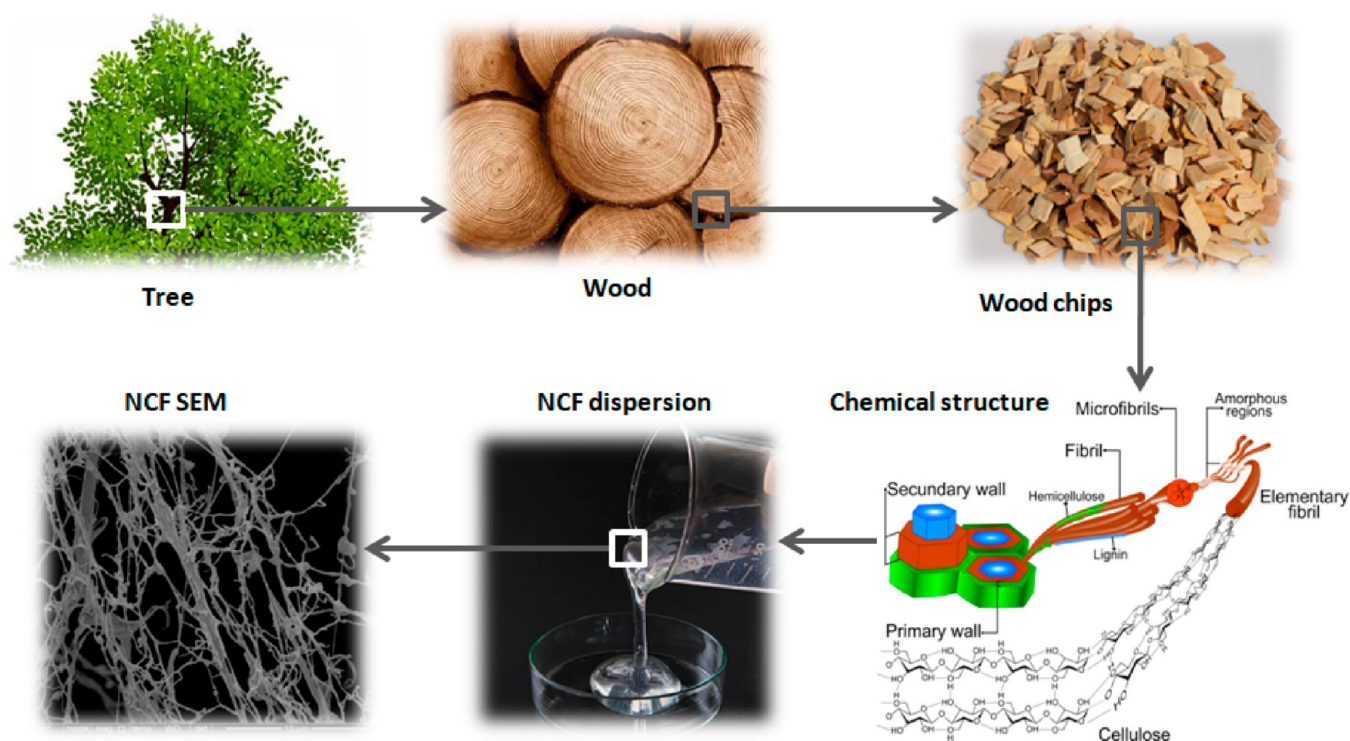


Figure 2. Illustration of cellulose extraction from tree. Adapted with permission from ref 41. Copyright 2018 MDPI.

The enhancement of foam stability can be achieved through inhibiting the foam destabilization (i.e., coarsening, drainage, or

coalescence). Coalescence can be effectively hampered if the films between bubbles are sufficiently thick, while liquid

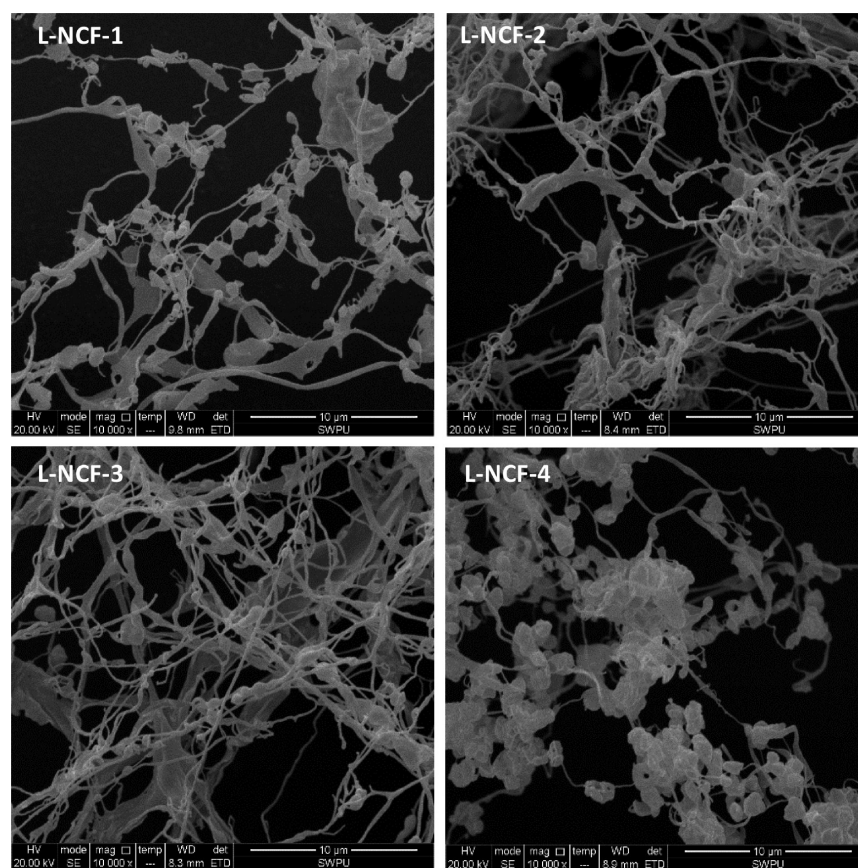


Figure 3. SEM images of four L-NCF samples and chemical unit.

drainage can be mitigated when foam stabilizers accumulate in the plateau borders or if they gel locally upon confinement caused by yield stress.^{18–20} The currently available foam stabilizers are categorized into two main groups, nanoparticles (NPs, silica, ash, aluminum, CaCO_3 , etc.)^{21–24} and polymeric materials (HPAM, xanthan, gel, etc.),^{25–27} as illustrated in Figure 1. Through adsorption and aggregation in foam films, NPs can increase film thickness and dilational viscoelasticity, which consequently decelerates liquid drainage and film thinning.^{15,28,29} In addition, the capability of the interface to bear in-plane shear has been recently demonstrated as a key factor in stabilizing droplets.³⁰ As for polymers, the predominant stabilizing mechanism is to significantly increase the bulk fluid viscosity of the foaming solution.

Nevertheless, the foams stabilized by NPs and polymers have not been widely accepted in oilfields because NPs are usually limited by unavailability and high-cost, while synthetic polymers (HPAM) may endanger the ecological environment due to the toxicity of the acrylamide monomer. Given these issues, economic and eco-friendly foam technologies must be developed to meet the requirements of the EOR industry today. Cellulose is a renewable material that is one of the most valuable biopolymers on the Earth. Figure 2 shows the scheme of cellulose extraction from raw materials.^{31–34} Not only is it the most abundant biomaterial, but it is a precursor for producing new chemicals, materials, and fuels.^{35–37} This fact motivated us to engineer its chemistry toward applications in the oil industry based on nanosize cellulose.^{4,5,38} In previous works, we reported the amphipathic nanocellulose that was produced by grafting 2-acrylamido-2-methylpropanesulfonic acid (AMPS) (hydrophilic) and ASA (hydrophobic) groups on the surface

simultaneously. It was observed that this kind of biomaterial was able to greatly strengthen foams, thus giving the foams superior stability especially in the presence of hydrocarbons.^{39,40} On the basis of our early works, for the purpose of further improving the economy of this technology, the chemical structure of the NCF was tailored, in which a small fraction of lignin was retained on the NCF surface together with some carboxyl groups. In this case, the manufacture of the amphipathic NCF can be noticeably simplified.

The primary focus of this work was to investigate the effect of the L-NCF structure on the interfacial stabilization of liquid foams in relation to both bulk and bubble scales. A series of L-NCF samples containing various contents of lignin and carboxyl groups were used for foaming with surfactants, after which the key parameters of foams, for example, foamability, foam stability, liquid fraction, drainage dynamics, bubble size, etc., were thoroughly investigated as a function of L-CNF chemical composition. The interfacial behaviors of the air/water interface including surface tension and dilational viscoelasticity were also examined in order to deeply reveal the underlying mechanisms. Furthermore, coreflooding experiments were conducted to study the transport of foam bubbles in porous media and correlate the foam bulk properties with the microscale flow behaviors. The results of this study supplement earlier findings in foam destabilization and provide alternative material for stabilizing foam film.

MATERIALS AND METHODS

Materials. The foaming agent, a blend of nonionic surfactant alkyl polyglycoside (APG) and anionic surfactant alpha olefin sulfonate (AOS) with a mass fraction of 35 wt %, was kindly supplied by Fukesi

Petroleum Technology Co., Ltd. The well-tailored L-NCF samples were provided by Tianjin Woodelf Biotechnology Co., Ltd. (Tianjin, China). Figure 3 shows the SEM images of four L-NCF samples. Table 1 summarizes the basic chemical properties of these samples (see the

Table 1. Basic Properties of Four L-NCF Samples

samples	content (wt %)		dimension (nm)		mass fraction in hydrogel (wt %)
	lignin ^a	carboxyl groups ^b	diameter	length	
L-NCF-1	15.5	1.12	2–5	800–1000	0.63
L-NCF-2	11.7	1.19	2–5	800–1000	0.70
L-NCF-3	8.66	1.29	2–5	800–1000	0.65
L-NCF-4	4.79	1.35	2–5	800–1000	0.92

^aThe content was determined using the method of TAPPI T 222 om-11(2011). ^bThe content was determined by titration.

Supporting Information for the surface morphology and EDX analysis of the samples, Figures S1 and S2). The synthetic brine with a salt concentration of 4.2 wt % consisting of NaCl (3.44 wt %), MgCl₂ (0.18 wt %), CaCl₂ (0.64 wt %), and Na₂SO₄ (0.018 wt %) was used throughout this work. The inorganic salts were purchased from Kelong Chemical Co., Ltd., China.

Scanning Electron Microscope Imaging (SEM). The micro-morphological features of the samples were observed by using a Quanta 450 scanning electron microscope at an excitation of 20 kV. A small amount of tested samples was first placed on a copper grid. The sample was evaporated using liquid nitrogen and then finally subjected to SEM observations. Afterward, the microgram images with different magnifications were recorded.

Foamability and Foam Stability. The foaming solutions were prepared by mixing the surfactant (0.4 wt %) with L-NCF samples (0.1 wt %) in brine at room temperature. All the solutions were mechanically stirred at 1000 rpm for 2 min to ensure homogeneity. A foam scanning apparatus (TECLIS-IT, France) was used in this work to evaluate the foam stability and foam texture. Figure 4 shows the schematic diagram of the foam scanner used in this work. By measuring the conductivity from certain ports (numbered 1 to 3) equipped on the foaming cylindrical column, the alterations of foam volume, liquid volume, and liquid fraction of foam films can be readily identified. A 60 mL aliquot of foaming solution was first loaded into the bottom of the column, after which nitrogen was injected at a constant flow rate of 120 mL/min to generate foam until two-third of the column volume was occupied by the generated foams. During the entire process, the experimental data were automatically recorded by the data acquisition system and then

subjected to the processing software for further analysis. All the experiments were performed at room temperature (20 °C) and atmospheric pressure.

Interfacial Dilational Rheology. The interfacial dilational rheology and surface tension were measured using a Tracker H tensiometer (Teclis, France).⁴² A small volume of the foaming solution was used to form a drop pending on the needle, after which a sinusoidal variation with a small amplitude ($\Delta A/A$, 10%) in the drop surface area was initiated by a piezoelectric pump (frequency, 0.1 Hz). The drop shape, volume, and area were subsequently read by the instrument camera and then analyzed using image software. All the measurements were conducted at room temperature (20 °C).

Coreflooding Experiment. Coreflooding experiments were performed to assess the foam generation in situ and flow behaviors of the foams in porous media. Table 2 lists the petrophysical properties of the core plugs used in this work. The procedures are as commonly reported. The coreholder was kept at a constant pressure of 0.5 MPa using a back-pressure regulator (BPR). In a typical flooding test, the core was first dried in an oven at 150 °C for overnight and then subjected to a vacuum (−0.1 MPa), after which the core was saturated with 4.2 wt % brine. Brine injection was resumed at a constant flow rate of 1.0 mL/min after the core plug was assembled in the coreholder to measure the permeability, pore volume (PV), and porosity of the core plug. After that, a foaming solution and nitrogen were co-injected into the core plug at a constant flow rate of 1.0 mL/min to displace the brine in place until the differential pressures (ΔP) across the core plug reached a steady state. A gas water ratio of 1:1 was used in this work to simply investigate the effect of L-CNF on foam stability in porous media. Brine injection was then resumed until the differential pressures (ΔP) stabilized again.

RESULTS AND DISCUSSION

Foamability and Foam Stability. As discussed earlier, foam is a thermodynamically metastable system, which would irreversibly evolve over time to minimize interfacial free energy of the system. The stability of bulk foams can be evaluated by the disjoining pressure (net results of repulsive forces and attractive forces), while in porous media foam stability is mainly determined by the limited capillary pressure.⁴³ These two key parameters are closely related to liquid film thickness, which can be represented by the liquid fraction of foams. As reported, the liquid fraction of foams plays the governing role in slowing down the rate of film rupture.⁴⁴ Commonly, liquid foams drain rapidly

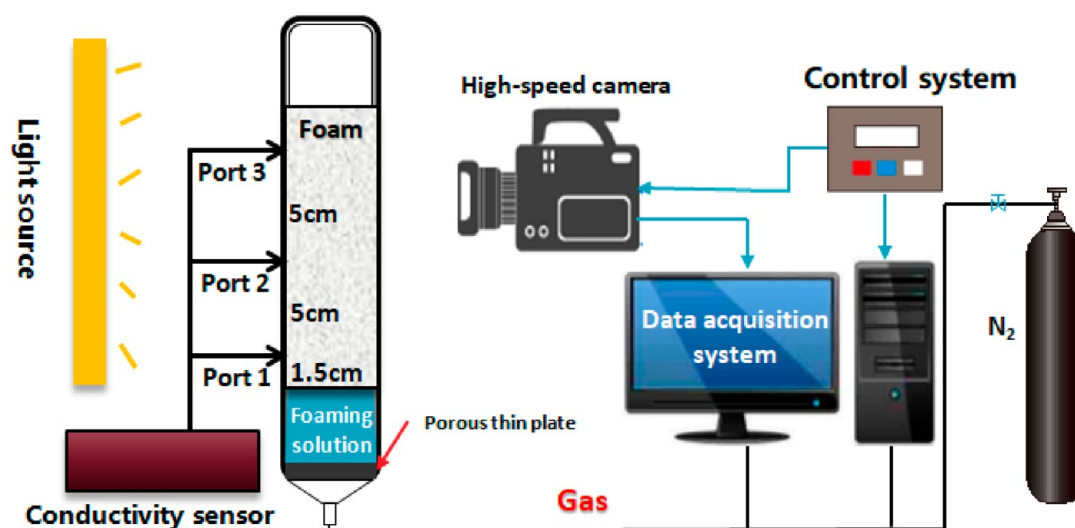


Figure 4. Schematic diagram of the foam scanner.

Table 2. Petrophysical Properties of the Core Plugs

core no.	length (cm)	diameter (cm)	permeability to brine (mD)	porosity (%)	average pore throat diameter (μm)	lithology
1	7.8	3.8	857.1	18.0	12.3	sandstone
2	7.8	3.8	862.9	17.9	12.4	
3	7.8	3.8	849.2	16.3	12.6	
4	7.8	3.8	857.3	17.2	12.6	
5	7.8	3.8	858.2	17.9	12.4	
6	7.8	3.8	857.2	19.0	12.0	
7	7.8	3.8	818.8	18.6	11.9	

under the impact of gravity until the liquid fraction reaches degrees less than a few percent.

The foamability and foam stability of the liquid foams containing different L-NCF were studied at the same formulation of 0.4 wt % surfactant and 0.1 wt % L-CNF. The entire process from bubbling to foam collapse was continuously monitored online by the foam scanner. Figure 5a–c plots the logarithmic liquid fraction of the produced foam systems with elapsed time from $t = 0$ to $t = 110$ min, during which the liquid fraction was observed to change intensively. As shown in Figure 5, the liquid fraction of the bubbling systems quickly increased until the peak values were reached in roughly 1 min, indicating the completion of the foaming process. Right after the peak, the liquid fraction gradually decreased over time in different rates under static conditions. The green curves were the surfactant foam in the absence of L-NCF. At the termination of foaming, the liquid fraction of the surfactant-only foam was found to decrease from port 1 to port 3 due to the effect of liquid gravity. The fast liquid drainage, as shown in Figure 5, especially panels b and c, suggested the instability of this foam.

In contrast to the “blank” foam, when L-NCF was combined with the surfactant for foaming together, the resultant foams became noticeably stable, as revealed by the reduced drainage rates (see Figure 5). At port 3, for example, the surfactant-only foam drained completely in 80 min, whereas for the L-NCF-3 stabilized foam more than 50% of liquid was still retained under the same experimental conditions. Furthermore, it was noted that the initial liquid fraction of all the generated foams at ports 1 and 2 were quite similar; however, at port 3, this value was much lower for the surfactant-only foam relative to the other foam systems. This result demonstrated that the addition of L-NCF to the surfactant could also enhance the liquid-carrying capacity of the foaming system. These observations indicated that incorporation of L-NCF in the foam film was able to largely “anchor” the film liquid, and thus obstructed gas transfer between bubbles (coarsening) thereby mitigating foam drainage (high stability). The mechanisms behind this will be discussed later. In summary, if one only considered the drainage rate, L-NCF-3 gave the produced foam the highest stability among four L-NCF samples.

Figure 6 depicts the liquid fraction of these five foam systems in the vertical column. The spatial liquid distributions from $t = 0$ to $t = 10$ min (resolution became quite low after 10 min) for the produced foams can be clearly identified. From Figure 6, the occurrence of the liquid drainage events with elapsed time were readily observed. It was confirmed that the addition of L-NCF yielded high resistance to liquid drainage for the foams especially L-NCF-3, which was proven to be the most appropriate candidate in our work.

Figure 7 shows the foam volume decay profiles for different foaming systems. As seen, the produced foams remained stable in the first 100 min roughly, after which a rapid decline in the

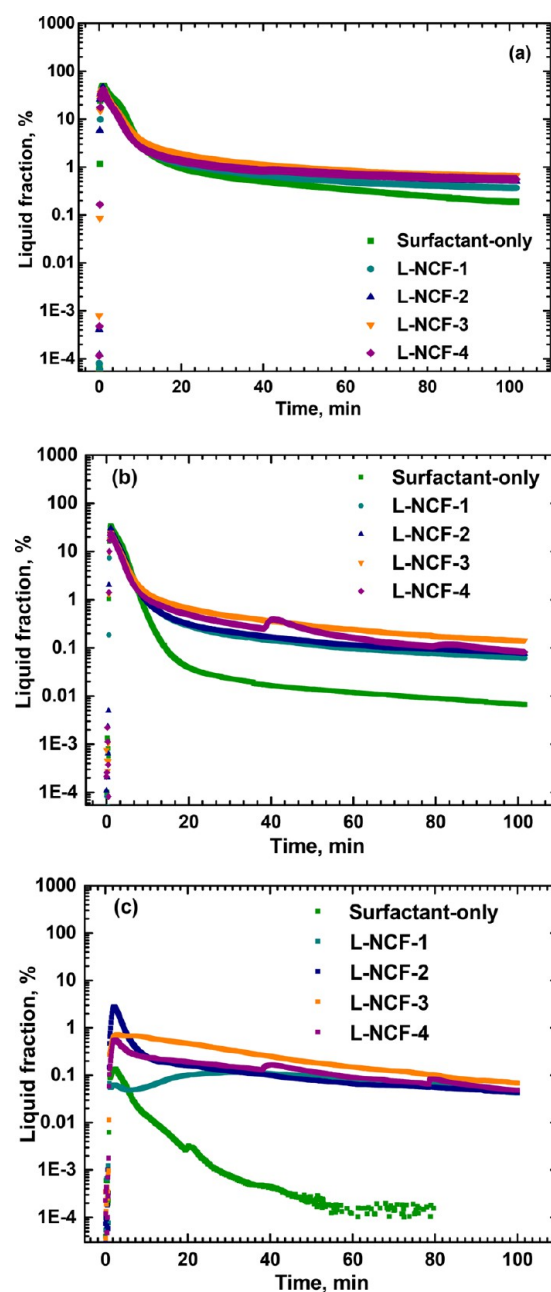


Figure 5. Liquid fraction curves of the generated foams plotted against time: (a) Port 1, (b) Port 2, and (c) Port 3.

foam volume occurred until the majority of the foams vanished in approximately 10 h. On the basis of the curves in Figure 7, the foam stability is ranked as the following, surfactant-only > L-NCF-3 > L-NCF-4 > L-NCF-1 > L-NCF-2. This order was surprisingly reversed for the surfactant-only foam in the drainage

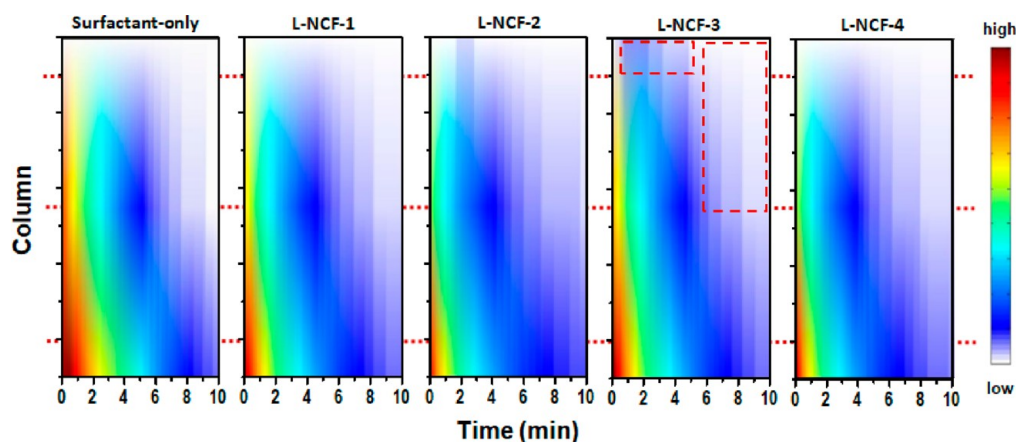


Figure 6. Maps of the liquid fraction of the produced foams in the vertical column. These maps were produced by Matlab software based on the liquid fraction evolution of the foams.

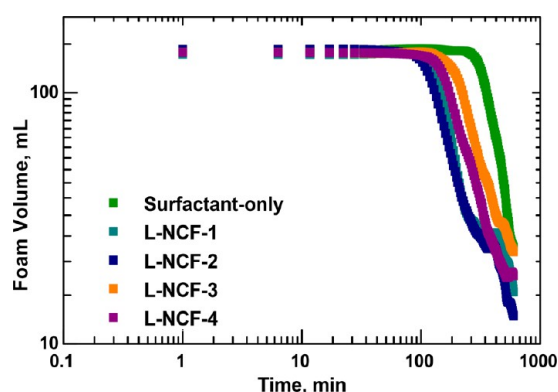


Figure 7. Foam volume decay profiles of different foam systems. X and Y axes were plotted in the logarithmic scale.

test (see Figure 5), in which this foam underwent the fastest drainage. The earlier collapse of the foams in the presence of L-NCF (1 to 4) was thought to be caused by the gravitational impact of the L-NCF samples, which caused the foam framework to easily rupture from the column top after the foams had severely drained. However, in porous media, the influence of L-NCF gravity on foam film can be neglected due to the limited pore size (nanometer to micrometer).

To further assess the stability of the foams, three parameters, namely foam expansion (FE), foam capacity (FC), and foam volume stability (FVS), were calculated after an experiment duration of 6 h by the following eqs 1–3. The obtained results were summarized in Table 3.

$$FE = \frac{V_{t\text{-foam}}}{V_{i\text{-liq}} - V_{f\text{-liq}}} \quad (1)$$

$$FC = \frac{V_{f\text{-foam}}}{V_{f\text{-gas}}} \quad (2)$$

$$FVS = \frac{V_{t\text{-foam}}}{V_{f\text{-foam}}} \quad (3)$$

where $V_{t\text{-foam}}$ is the volume of foam at the end of the foaming process, $V_{i\text{-liq}}$ is the initial liquid volume, $V_{f\text{-liq}}$ is the final liquid volume, $V_{f\text{-foam}}$ is the final foam volume, and $V_{f\text{-gas}}$ is the final gas volume.

Table 3. FE, FC, and FVS Values of Different Foam Systems. These Values Were Calculated by the Foam Scanner Automatically

samples	foam volume (mL)	FE	FC	FVS
surfactant-only	157	6.8	1.35	2.23
L-NCF-1	157	6.7	1.35	9.07
L-NCF-2	158	6.7	1.36	9.39
L-NCF-3	160	6.9	1.39	11.58
L-NCF-4	149	10.1	1.28	9.68

As shown in Table 3, the FE and FC values of the foams were fairly close, but the FVS values, which determine the foam stability in bulk, varied significantly among the different samples. After the addition of L-NCF, the stability of the resultant foams was improved up to 5.2 times based on the surfactant-only foam, verifying the superior foam stabilizing effect of the proposed materials. These results are in agreement with the observations in the drainage tests (see Figure 5).

Bubble Number and Size Evolution. In this section, the stability of these foams was evaluated at the bubble scale. The foam images were taken from port 2 at different times attempting to visually observe the bubble evolution in detail. Figure 8 shows qualitatively the state of the bubbles in different foam systems from the onset of the experiments ($t = 1\text{--}20$ min). It is clear that fine-textured bubbles with spherical configuration and uniform size distribution were produced initially, and then slowly distorted into polyhedra with liquid drainage.

With the assistance of the image analysis system, the normalized number of bubbles was determined as a function of time to quantify the dynamics and characteristics of the foams (see Figure 9a). This result is expected to supplement previous findings and provide insight into the foam stability at the microscale. As Figure 9a shows, the normalized number of bubbles quickly decreased with time caused by the net effect of coarsening and coalescence. The curves also demonstrated that after L-NCF was added, the decreasing rate of the bubble numbers was slowed mainly due to the mitigated liquid drainage (see Figure 5). This consequently led to the increase of the average distance between foam bubbles and finally high foam stability.

The degree of foam coarsening can also be determined qualitatively from the evolution of bubble size with time. Figure 9b plots the maximum bubble size of different foams with time. It was found that the presence of L-NCF in the foaming solution

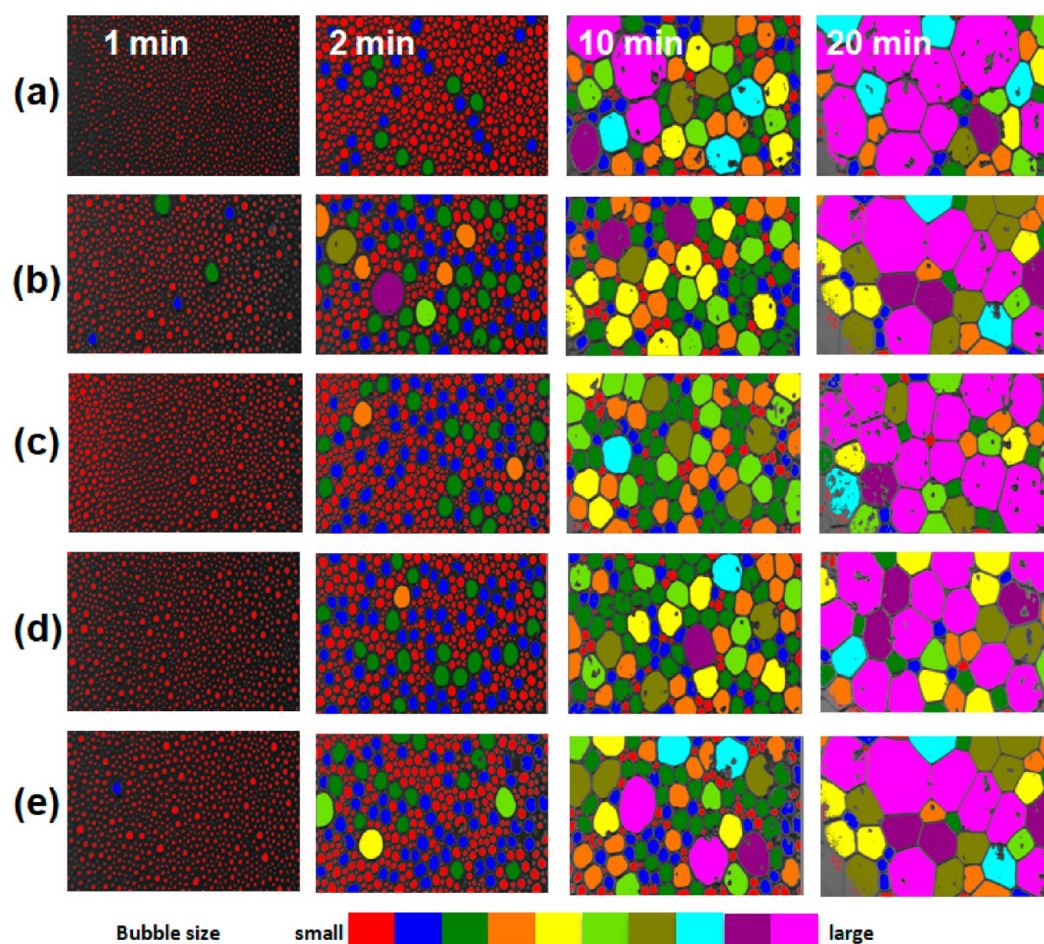


Figure 8. Images of different foam bubbles with time: (a) surfactant-only, (b) L-NCF-1, (b) L-NCF-2, (c) L-NCF-3, and (d) L-NCF-4. The color bar at the bottom of the images indicates the bubble size.

increased the initial bubble size. This occurred because the addition of L-NCF increased the viscosity of the solution and therefore raised the dissipated energy in foaming.⁴⁵ In contrast, the surfactant-only foam possessed the smallest initial bubble of 0.02 mm among all the tested systems. However, this foam bubble experienced significant coarsening in 20 min leading the bubble size to be 580 times that of the initial state. Consistent with our earlier observations, the addition of L-NCF, especially L-NCF-3, hindered the bubble size growth and produced stable foams.

Coreflooding Experiment. After the static tests, a series of coreflooding experiments were conducted to investigate the behaviors of bubble transport and retention in porous media, and then relate them to the foam interfacial properties. The injection scheme and differential pressures (ΔP) across the core plugs were plotted against the injected PV of fluids in Figure 10. Table 4 summarizes the resistance factor (RF) and residual resistance factor (RRF) obtained from these experiments. The core plugs had comparable petrophysical properties as indicated in Table 2.

Note that for the seven core plugs the injection of brine produced very low ΔP ; nevertheless, when the injection was switched to foam, the magnitude of the produced ΔP steeply increased for all the cases and then reached equilibrium after approximately 2.0 PV injection. When the brine injection was resumed, as revealed in Figure 10, the generated ΔP slowly declined and finally stabilized. The established ΔP in the

resumed brine injection phase was mainly caused by the trapped bubbles (Jamin effect) and L-NCF retention as observed from the ΔP profile of the foaming solution. The evolution of the ΔP upon PV indicated that the L-NCF stabilized foams in our work can properly flow through the core plugs without any plugging issue (see Figure 10). Injectivity is one of the most important criteria for screening chemicals. As anticipated, under identical experimental conditions, the L-NCF stabilized foams produced notably higher ΔP than the surfactant-only foam, confirming the stability of these foams in porous media (see Figure S3). This result also verified the dependence of foam flowing behaviors in porous media on bulk foam stability.

Air Water Interfacial Properties. The interfacial stabilization of surfactant foams with the presence of L-NCF has been conclusively evidenced at the bulk and bubble scales. The focus of this section was given to the interfacial properties of the foams with an aim to understand the interactions between the surfactant and L-NCF within the air water interface.

Figure 11 plots the surface tension of different systems over the measuring time. In this time interval, the surface tension was found to slightly change and mainly varied from 13 to 18 mN/m between different systems. The addition of L-NCF into the surfactant solution reduced the surface tension up to 5 mN/m (L-NCF-3), most likely caused by the surface activity of L-NCF generated by its distinctive chemical structure (both hydrophobic and hydrophilic groups on the surface). The facilitated adsorption of the surfactant and L-NCF at the air water interface

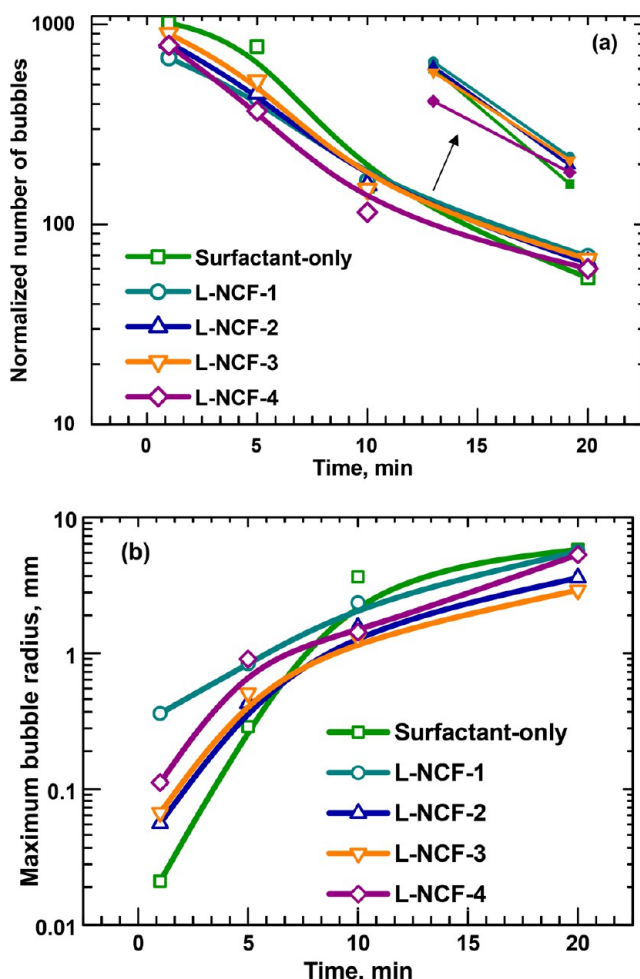


Figure 9. (a) Normalized number of bubbles in the column as a function of time; (b) maximum bubble size as a function of time. Y axis was plotted in the logarithmic scale.

finally led to the observed results. However, it should be noted that the surface tension reduction by L-NCF was insignificant; thus, it was not the main reason for foam stability.

We have also compared the interfacial dilational rheology of the foams before and after stabilization by L-NCF (Supporting Information. Images taken in the measurements, Figure S3). Figure 12 shows the modulus of different foams. In general, as depicted in Figure 12a, the presence of L-NCF in the foam film promoted the surfactant to build up a viscoelastic interface due to the cohesive hydrophobic interaction between the surfactant and L-NCF as claimed by Dan et al. and Tardy et al.^{46,47} Figure 12 panels b and c plot the respective elastic and viscous moduli of the systems. Note that the magnitude of the elastic moduli of the measured systems was higher than the viscous moduli, indicating the elastic behavior of the newly formed interface. In addition, as indicated in Figure 12 panels b and c, the addition of L-NCF mainly improved the elasticity of the interface, whereas the interfacial viscosity was not significantly changed. This result can be related to the rigidity of the nanocellulose chains (less flexible than polyacrylamide, PAM), which thus imparts an elastic behavior to the NCF. The rheological properties of NCF have been extensively investigated in the literature as reviewed previously.^{48,49}

The elastic air water interface can help foams combat coarsening due to its mechanical properties. Meinders and

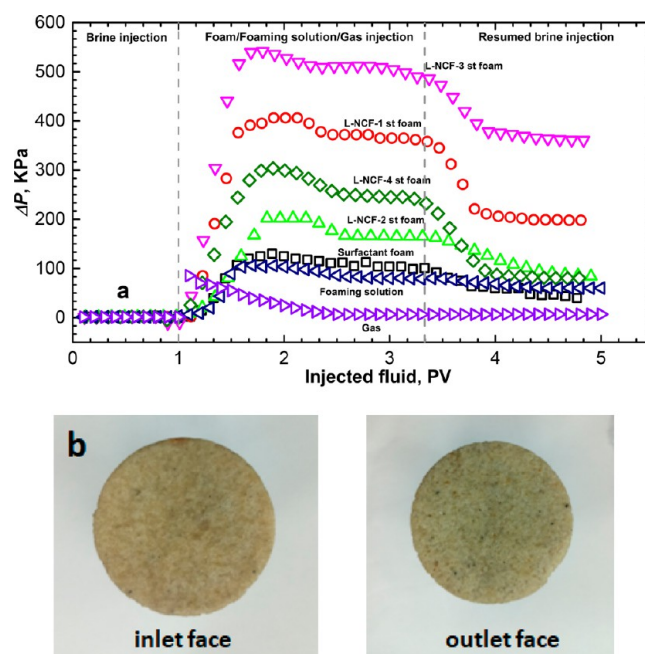


Figure 10. (a) Differential pressure (ΔP) curves plotted with the injected PV of fluids; (b) images of the inlet face and outlet face of the core plug at the termination of foam injection (L-NCF-3). No filtered L-NCF cake was formed.

Table 4. RF and RRF Produced during the Coreflooding Experiment

samples	RF ^a	RRF ^b
surfactant-only	56	28
L-NCF-1	186	99.5
L-NCF-2	81	42
L-NCF-3	251	182.5
L-NCF-4	122.5	41
foaming solution (L-NCF-3 and surfactant)	75.4	61.3
gas		5.8

^aRF is defined as the ΔP of foam injection divided by ΔP of the first brine injection. ^bRRF is defined as the ΔP of resumed brine injection divided by ΔP of the first brine injection.

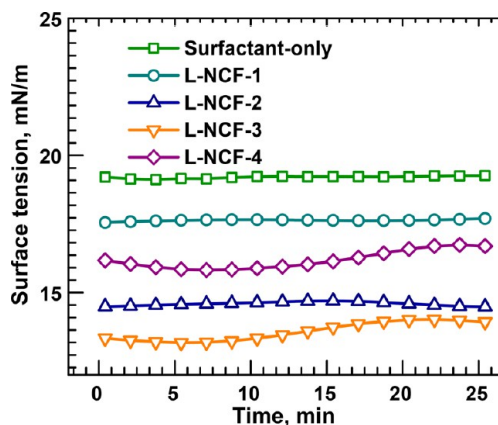


Figure 11. Dynamic surface tension of different foaming systems as a function of time.

Vliet claimed that the Ostwald ripening could be mitigated by increasing the compression elastic modulus of the monolayer. When the elastic modulus achieved a certain value, the Ostwald

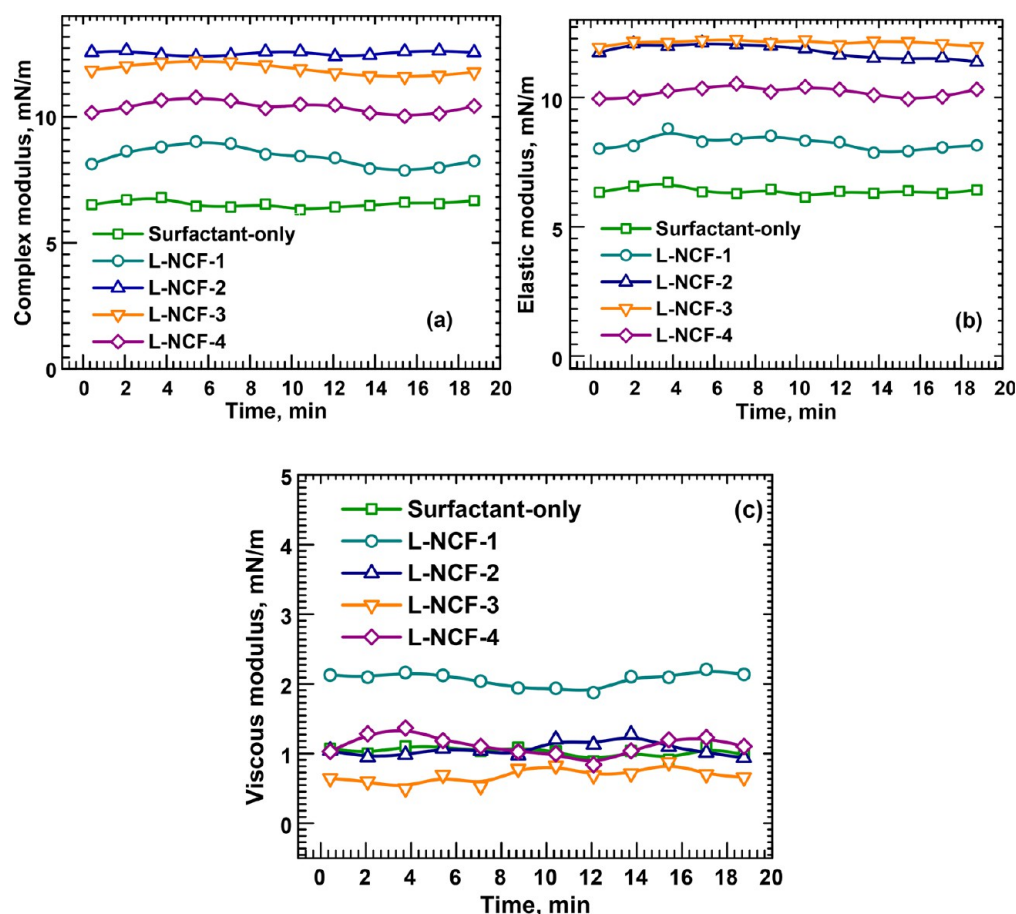


Figure 12. (a) Dilational complex viscoelasticity modulus; (b) elastic modulus; and (c) viscous modulus of different systems.

ripening process stopped.^{50,51} Hence, the elastic interface of the L-NCF stabilized foams was supposed to decrease the permeability of the film to gas, which thus inhibited gas diffusion between bubbles. In addition to the arrest of coarsening, the improved interfacial elasticity was capable of stabilizing water and reducing the liquid drainage rate (see Figure 5). Apparently, the intensity of the interaction between L-NCF-3 and the surfactant was higher than that of the other samples.

SEM images of the surfactant/L-NCF mixtures are shown in Figure 13. Compared to the original states (see Figure 3), it was found that the framework of the mixtures became significantly thick and dense. The SEM observations supplied additional evidence of the intermolecular interaction responsible for the elastic behavior of the interface. On the basis of the obtained results, it can be inferred that the surfactant/L-NCF interaction within the air water interface was the predominant mechanism for foam stability.¹⁸

SUMMARY AND PROSPECTS

In summary, we demonstrated that L-NCF was promising as a stabilizer for the foam interface, and the resulting foam could be used for robust EOR as a green alternative technology. The predominant stabilizing mechanism was the interaction between surfactant and L-NCF, which led the closed-packed film to be strengthened further. The generated foams therefore had combined resistance to three types of destabilization mechanisms: coarsening, drainage, and coalescence, as mentioned earlier.

As reported,³⁸ the film stabilizing effect of the nanocellulose based materials was also due to the potential hydrogen bond formed between water and nanocellulose as a result of sustainable $-OH$ groups on the surface. By this point, it is understandable that there exists an optimal content of lignin on the L-NCF surface for foam stabilization. First of all, a significant interaction between the surfactant and L-NCF takes place only for the highly hydrophobic L-NCF (high lignin contents) sample when the forces of the hydrophobic interaction overcome the electrostatic repulsion between the negatively charged species. Second, the content of the hydrophobic segment needs to be coordinated since it poses a detrimental effect on the formation of hydrogen bonding. Therefore, in our work, the sample with 8.66 wt % of lignin and 1.29 wt % carboxyl groups (L-NCF-3) was proven to be the most effective L-NCF for stabilizing the interface. Further investigation into the interactions is in progress in our group.

The results of the coreflooding experiment revealed that the L-NCF stabilized foams (only 0.1 wt %) can produce noticeably large RF and RRF values, which are desirable for modifying the mobility ratio between the displacing phase and displaced phase. It is believed that this result was also related to the increased elasticity of the interface. A number of studies have shown that the critical capillary number, C_a ($C_a = \mu v / \sigma$), for bubble or droplet breakup increases with the interfacial elasticity in pore throats,^{52–54} because viscous (drag) forces become large enough to overcome the capillary pressure threshold at the critical C_a . This would result in a large ΔP or flow resistance for

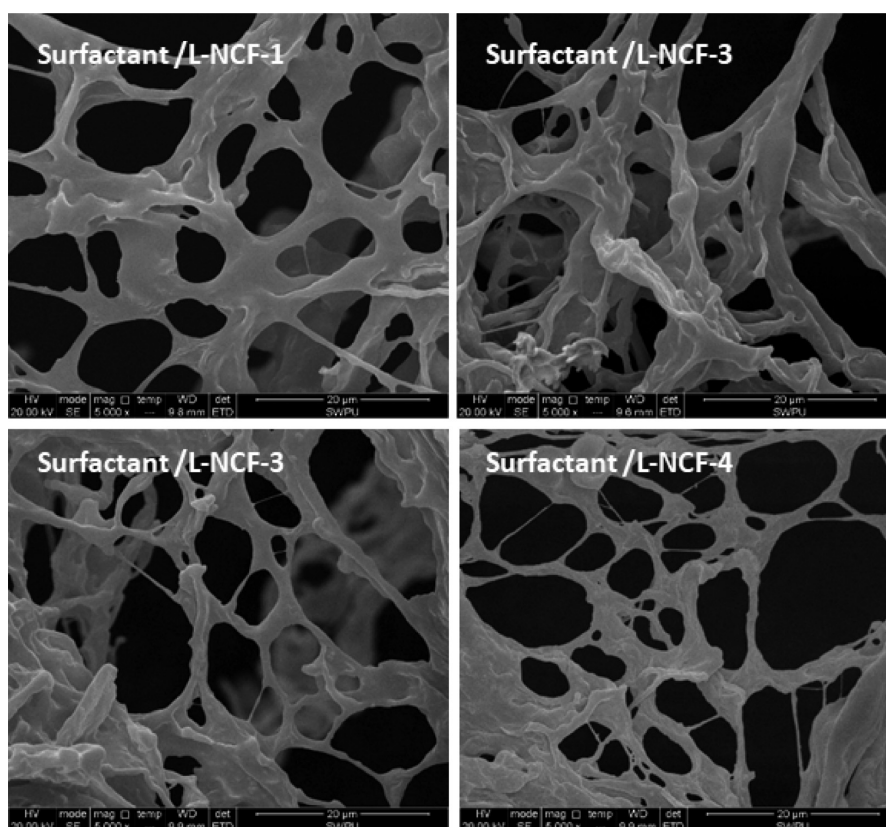


Figure 13. SEM images of the surfactant/L-NCF mixtures.



Figure 14. Utilization of cellulose materials in different industries. Adapted with permission from ref 55. Copyright 2012 OECD.

the L-NCF stabilized foams when their bubbles converged into the pore throat.

With the maturity of the worldwide oilfields, significant research efforts have been directed to enhanced or improved oil recovery (EOR or IOR). Therefore, the consumption of oilfield chemicals keeps growing, especially in China. This fact provides

the motivation for petroleum engineers to develop eco-friendly, large-quantity available, and economic materials in order to meet the requirements of oilfield-scale production. Nano-cellulose has been intensively used in various areas as summarized in Figure 14,⁵⁵ which also promotes the utilization of this emerging material in the oil production industry.

Although the technical feasibility of nanocellulose in EOR has been preliminarily demonstrated, the manufacturing cost still limits the field-scale use especially in the depressed energy market. Substantial efforts should be made to further reduce the cost in the next stage in terms of raw materials and energy consumption of manufacturing, etc.

CONCLUSION

A series of nanocellulose fibrils containing lignin (L-NCF) were successfully designed and used to stabilize the air water interface of foam systems for potential application in oil recovery process. The addition of L-NCF into the surfactant significantly mitigated the liquid drainage of the foams. The stability of the resultant foams was improved up to 5 times compared to that of the surfactant-only foam. The hydrophobic interaction between lignin (the hydrophobic segment on nanocellulose) and the surfactant constructed an elastic interface, which, in turn, inhibited the occurrence of coarsening, drainage, and coalescence. The elastic interface gave the foams superior ability in mobility control and made them excellent candidates for robust oil recovery processes. The lignin content strongly determined the interfacial stabilizing effect of L-NCF due to the competition between hydrophobic and hydrophilic interactions within the interface. Therefore, the chemical structure of L-NCF should be well tailored to optimize the foam stability.

ASSOCIATED CONTENT

Supporting Information

The Supporting Information is available free of charge on the ACS Publications website at DOI: 10.1021/acssuschemeng.9b01249.

Surface morphologies; EDX spectra; measurements of air water interfacial dilational viscoelasticity (PDF)

AUTHOR INFORMATION

Corresponding Author

*Email: bwei@swpu.edu.cn.

ORCID

Bing Wei: 0000-0003-2243-0995

Colin Wood: 0000-0001-6160-0112

Notes

The authors declare no competing financial interest.

ACKNOWLEDGMENTS

The authors gratefully acknowledge the financial support of National Natural Science Foundation of China (51804264) and Youth Science and Technology Innovation Team of SWPU (2017CXTD04). The authors also thank the anonymous reviewers for their valuable comments.

REFERENCES

- (1) Hirasaki, G. J. The Steam-Foam Process. *JPT, J. Pet. Technol.* **1989**, 41 (5), 449–456.
- (2) Zha, J.; Batisse, N.; Claves, D.; Dubois, M.; Frezet, L.; Kharitonov, A. P.; Alekseiko, L. N. Superhydrophobicity via gas-phase monomers grafting onto carbon nanotubes. *Prog. Surf. Sci.* **2016**, 91 (2), 57–71.
- (3) Jin, H. J.; Zhou, W. Z.; Cao, J.; Stoyanov, S. D.; Blijdenstein, T. B. J.; de Groot, P. W. N.; Arnaudov, L. N.; Pelan, E. G. Super stable foams stabilized by colloidal ethyl cellulose particles. *Soft Matter* **2012**, 7 (8), 2194–2205.
- (4) Zhang, Y.; Wang, S. C.; Zhou, J. R.; Zhao, R. Y.; Benz, G.; Tcheimou, S.; Meredith, J. C.; Behrens, S. H. Interfacial activity of

nonamphiphilic particles in fluid-fluid interfaces. *Langmuir* **2017**, 33 (18), 4511–4519.

- (5) Tye, Y. Y.; Lee, K. T.; Wan Abdullah, W. N.; Leh, C. P. The world availability of non-wood lignocellulosic biomass for the production of cellulosic ethanol and potential pretreatments for the enhancement of enzymatic saccharification. *Renewable Sustainable Energy Rev.* **2016**, 60, 155–172.
- (6) Wei, B.; Ning, J.; Mao, R.; Wang, Y.; Xu, X.; Bai, M. Rational design and fabrication of an alkali-induced O/W emulsion stabilized with cellulose nanofibrils (CNFs): implication for eco-friendly and economic oil recovery application. *Soft Matter* **2019**, 15, 4026–4034.
- (7) Andrianov, A.; Farajzadeh, R.; Mahmoodi Nick, M. M.; Talanana, M.; Zitha, P. L. J. Immiscible Foam for Enhancing Oil Recovery: Bulk and Porous Media Experiments. *Ind. Eng. Chem. Res.* **2012**, 51, 2214–2226.
- (8) Farajzadeh, R.; Andrianov, A.; Zitha, P. L. J. Investigation of Immiscible and Miscible Foam for Enhancing Oil Recovery. *Ind. Eng. Chem. Res.* **2010**, 49 (4), 1910–1919.
- (9) Hadjiiski, A.; Tcholakova, S.; Denkov, N. D.; Durbut, P.; Broze, G.; Mehreteab, A. Effect of Oily Additives on Foamability and Foam Stability. 2. Entry Barriers. *Langmuir* **2001**, 17 (22), 7011–7021.
- (10) Arnaudov, L.; Denkov, N. D.; Surcheva, I.; Durbut, P.; Broze, G.; Mehreteab, A. Effect of Oily Additives on Foamability and Foam Stability. 1. Role of Interfacial Properties. *Langmuir* **2001**, 17 (22), 6999–7010.
- (11) Farajzadeh, R.; Andrianov, A.; Krastev, R.; Hirasaki, G. J.; Rossen, W. R. Foam-oil interaction in porous media: Implications for foam assisted enhanced oil recovery. *Adv. Colloid Interface Sci.* **2012**, 183–184, 1–13.
- (12) Gauglitz, P. A.; St. Laurent, C. M.; Radke, C. J. Experimental determination of gas-bubble breakup in a constricted cylindrical capillary. *Ind. Eng. Chem. Res.* **1988**, 27 (7), 1282–1291.
- (13) Hosseini-Nasab, S. M.; Zitha, P. L. J. Investigation of Chemical-Foam Design as a Novel Approach toward Immiscible Foam Flooding for Enhanced Oil Recovery. *Energy Fuels* **2017**, 31 (10), 10525–10534.
- (14) Shojaei, M. J.; Osei-Bonsu, K.; Grassia, P.; Shokri, N. Foam Flow Investigation in 3D-Printed Porous Media: Fingering and Gravitational Effects. *Ind. Eng. Chem. Res.* **2018**, 57 (21), 7275–7281.
- (15) Wu, Y.; Fang, S.; Zhang, K.; Zhao, M.; Jiao, B.; Dai, C. Stability Mechanism of Nitrogen Foam in Porous Media with Silica Nanoparticles Modified by Cationic Surfactants. *Langmuir* **2018**, 34 (27), 8015–8023.
- (16) Micheau, C.; Bauduin, P.; Diat, O.; Faure, S. Specific salt and pH effects on foam film of a pH sensitive surfactant. *Langmuir* **2013**, 29 (27), 8472–8481.
- (17) Gauteplass, J.; Chaudhary, K.; Kovscek, A. R.; Fernø, M. A. Pore-level foam generation and flow for mobility control in fractured systems. *Colloids Surf., A* **2015**, 468, 184–192.
- (18) Rio, E.; Drenckhan, W.; Salonen, A.; Langevin, D. Unusually stable liquid foams. *Adv. Colloid Interface Sci.* **2014**, 205 (12), 74–86.
- (19) Ramanathan, M.; Müller, H. J.; Möhwald, H.; Krastev, R. Foam films as thin liquid gas separation membranes. *ACS Appl. Mater. Interfaces* **2011**, 3 (3), 633–637.
- (20) Schulze-Zachau, F.; Braunschweig, B. R. Structure of Polystyrenesulfonate/Surfactant Mixtures at Air-Water Interfaces and Their Role as Building Blocks for Macroscopic Foam. *Langmuir* **2017**, 33 (14), 3499–3508.
- (21) Toor, A.; Lamb, S.; Helms, B.; Russell, T. P. Reconfigurable Microfluidic Droplets Stabilized by Nanoparticle Surfactants. *ACS Nano* **2018**, 12 (3), 2365–2372.
- (22) Khalil, M.; Jan, B. M.; Tong, C. W.; Berawi, M. A. Advanced nanomaterials in oil and gas industry: Design, application and challenges. *Appl. Energy* **2017**, 191, 287–310.
- (23) Yang, W.; Wang, T.; Fan, Z. Highly stable foam stabilized by alumina nanoparticles for EOR: Effects of sodium cumenesulfonate and electrolyte concentrations. *Energy Fuels* **2017**, 31 (9), 9016–9025.
- (24) Singh, R.; Mohanty, K. K. Synergy between Nanoparticles and Surfactants in Stabilizing Foams for Oil Recovery. *Energy Fuels* **2015**, 29 (2), 467–479.

- (25) Jones, M. N. The interaction of sodium dodecyl sulfate with polyethylene oxide. *J. Colloid Interface Sci.* **1967**, 23 (1), 36–42.
- (26) Philippova, O. E.; Hourdet, D.; Audebert, R.; Khokhlov, A. R. Interaction of Hydrophobically Modified Poly(acrylic acid) Hydrogels with Ionic Surfactants. *Macromolecules* **1996**, 29 (8), 2822–2830.
- (27) Zhao, G.; Dai, C.; Zhang, Y.; Chen, A.; Yan, Z.; Zhao, M. Enhanced foam stability by adding comb polymer gel for in-depth profile control in high temperature reservoirs. *Colloids Surf., A* **2015**, 482, 115–124.
- (28) Sun, Q.; Li, Z.; Li, S.; Jiang, L.; Wang, J.; Wang, P. Utilization of Surfactant-Stabilized Foam for Enhanced Oil Recovery by Adding Nanoparticles. *Energy Fuels* **2014**, 28 (4), 2384–2394.
- (29) Wu, Y.; Wang, R.; Dai, C.; Xu, Y.; Yue, T.; Zhao, M. Precisely Tailoring Bubble Morphology in Microchannel by Nanoparticles Self-assembly. *Ind. Eng. Chem. Res.* **2019**, 58 (9), 3707–3713.
- (30) Emile, J.; Salonen, A.; Dollet, B.; Saint-Jalmes, A. A systematic and quantitative study of the link between foam slipping and interfacial viscoelasticity. *Langmuir* **2009**, 25 (23), 13412–13418.
- (31) Eichhorn, S. J.; Dufresne, A.; Aranguren, M.; Marcovich, N. E.; Capadona, J. R.; Rowan, S. J.; Weder, C.; Thielemans, W.; Roman, M.; Renneckar, S.; et al. Review: current international research into cellulose nanofibres and nanocomposites. *J. Mater. Sci.* **2010**, 45 (1), 1–33.
- (32) Habibi, Y.; Lucia, L. A.; Rojas, O. J. Cellulose Nanocrystals: Chemistry, Self-Assembly, And Applications. *Chem. Rev.* **2010**, 110 (6), 3479–3500.
- (33) Wang, Z.; Lin, W.; Song, W. Liquid product from hydrothermal treatment of cellulose by direct GC/MS analysis. *Appl. Energy* **2012**, 97 (9), 56–60.
- (34) Sathvika, T.; Manasi; Rajesh, V.; Rajesh, N. Microwave assisted immobilization of yeast in cellulose biopolymer as a green adsorbent for the sequestration of chromium. *Chem. Eng. J.* **2015**, 279, 38–46.
- (35) Magalhães, W. L.; Cao, X.; Lucia, L. A. Cellulose nanocrystals/cellulose core-in-shell nanocomposite assemblies. *Langmuir* **2009**, 25 (22), 13250–13257.
- (36) Janardhnan, S.; Sain, M. M. Isolation of cellulose microfibrils - An enzymatic approach. *Bioresour.* **2006**, 1 (2), 176–188.
- (37) Klemm, D.; Schumann, D.; Kramer, F.; Hessler, N.; Hornung, M.; Schmauder, H. P.; Marsch, S. Nanocelluloses as Innovative Polymers in Research and Application. *Adv. Polym. Sci.* **2006**, 205, 49–96.
- (38) Wei, B.; Li, H.; Li, Q.; Wen, Y.; Sun, L.; Wei, P.; Pu, W.; Li, Y. Stabilization of Foam Lamella Using Novel Surface-Grafted Nanocellulose-Based Nanofluids. *Langmuir* **2017**, 33 (21), 5127–5139.
- (39) Li, Q.; Wei, B.; Lu, L.; Li, Y.; Wen, Y.; Pu, W.; Li, H.; Wang, C. Investigation of physical properties and displacement mechanisms of surface-grafted nano-cellulose fluids for enhanced oil recovery. *Fuel* **2017**, 207, 352–364.
- (40) Wei, B.; Li, Q.; Jin, F. Y.; Li, H.; Wang, C. The Potential of a Novel Nanofluid in Enhancing Oil Recovery. *Energy Fuels* **2016**, 30 (4), 2882–2891.
- (41) Aadland, R. C.; Dziuba, C. J.; Heggset, E. B.; Syverud, K.; Torsæter, O.; Holt, T.; Gates, I. D.; Bryant, S. L. Identification of Nanocellulose Retention Characteristics in Porous Media. *Nanomaterials* **2018**, 8 (7), 547.
- (42) Ligiero, L. M.; Bouriat, P.; Dicharry, C.; Passadeboup, N.; Lalli, P. M.; Rodgers, R. P.; Barrèremangote, C.; Giusti, P.; Bouysiere, B. Characterization of crude oil Interfacial Material isolated by the wet silica method. Part I-Gel Permeation Chromatography Inductively Coupled Plasma High Resolution Mass Spectrometry analysis. *Energy Fuels* **2017**, 31, 1065–1071.
- (43) Farajzadeh, R.; Andrianov, A.; Krastev, R.; Hirasaki, G. J.; Rossen, W. R. Foam-oil interaction in porous media: Implications for foam assisted enhanced oil recovery. *Adv. Colloid Interface Sci.* **2012**, s183–184, 1–13.
- (44) Carn, F.; Colin, A.; Pitois, O.; Vignes-Adler, M.; Backov, R. Foam drainage in the presence of nanoparticle-surfactant mixtures. *Langmuir* **2009**, 25 (14), 7847–7856.
- (45) Li, S.; Xiang, W.; Jarvinen, M.; Lappalainen, T.; Salminen, K.; Rojas, O. J. Interfacial Stabilization of Fiber-Laden Foams with Carboxymethylated Lignin toward Strong Nonwoven Networks. *ACS Appl. Mater. Interfaces* **2016**, 8 (30), 19827–19835.
- (46) Dan, A.; Gochev, G.; Miller, R. Tensiometry and dilational rheology of mixed beta-lactoglobulin/ionic surfactant adsorption layers at water/air and water/hexane interfaces. *J. Colloid Interface Sci.* **2015**, 449, 383–391.
- (47) Tardy, B. L.; Yokota, S.; Ago, M.; Xiang, W.; Kondo, T.; Bordes, R.; Rojas, O. J. Nanocellulose-surfactant interactions. *Curr. Opin. Colloid Interface Sci.* **2017**, 29, 57–674.
- (48) Lundahl, M. J.; Berta, M.; Ago, M.; Stading, M.; Rojas, O. J. Shear and extensional rheology of aqueous suspensions of cellulose nanofibrils for biopolymer-assisted filament spinning. *Eur. Polym. J.* **2018**, 109, 367–378.
- (49) Nechyporchuk, O.; Belgacem, M. N.; Pignon, F. Current Progress in Rheology of Cellulose Nanofibril Suspensions. *Biomacromolecules* **2016**, 17 (7), 2311–2320.
- (50) Meinders, M. B. J.; van Vliet, T. The role of interfacial rheological properties on Ostwald ripening in emulsions. *Adv. Colloid Interface Sci.* **2004**, 108 (10), 119–126.
- (51) Georgieva, D.; Schmitt, V.; Leal-Calderon, F.; Langevin, D. On the possible role of surface elasticity in emulsion stability. *Langmuir* **2009**, 25 (10), 5565–5573.
- (52) Cardinaels, R.; Vananroye, A.; Puyvelde, P. V.; Moldenaers, P. Breakup Criteria for Confined Droplets: Effects of Compatibilization and Component Viscoelasticity. *Macromol. Mater. Eng.* **2011**, 296 (3–4), 214–222.
- (53) Aggarwal, N.; Sarkar, K. Deformation and breakup of a viscoelastic drop in a Newtonian matrix under steady shear. *J. Fluid Mech.* **2007**, 584 (584), 1–21.
- (54) Wei, B.; Wu, R.; Lu, L.; Ning, X.; Xu, X.; Wood, C. D.; Yang, Y. Influence of Individual Ions on Oil/Brine/Rock Interfacial Interactions and Oil Water Flow Behaviors in Porous Media. *Energy Fuels* **2017**, 31, 12035–12045.
- (55) Crotofino, R. Presented at The economic impact of Nano-cellulose, *International Symposium on Assessing the Economic Impact of Nanotechnology*, Washington DC, March 27–28; Washington DC, 2012.